remote sensing

MDPI

Article

A New Fast and Low-Cost Photogrammetry Method for the Engineering Characterization of Rock Slopes

Mirko Francioni [1,*], Matteo Simone [1], Doug Stead [2], Nicola Sciarra [1], Giovanni Mataloni [3] and Fernando Calamita [1]

[1] Department of Engineering and Geology, University "G. d'Annunzio" of Chieti-Pescara, 66100 Chieti, Italy; mat.sim.93@hotmail.it (M.S.); nsciarra@unich.it (N.S.); calamita@unich.it (F.C.)
[2] Department of Earth Sciences, Simon Fraser University, Burnaby, BC V5A 1S6, Canada; dstead@sfu.ca
[3] Department of Architecture, University "G. d'Annunzio" of Chieti-Pescara, 66100 Chieti, Italy; giovanni.mataloni@unich.it
* Correspondence: mirko.francioni@unich.it

Received: 8 April 2019; Accepted: 23 May 2019; Published: 28 May 2019

Abstract: Digital photogrammetry (DP) represents one of the most used survey techniques in engineering geology. The availability of new high-resolution digital cameras and photogrammetry software has led to a step-change increase in the quality of engineering and structural geological data that can be collected. In particular, the introduction of the structure from motion methodology has led to a significant increase in the routine uses of photogrammetry in geological and engineering geological practice, making this method of survey easier and more attractive. Using structure from motion methods, the creation of photogrammetric 3D models is now easier and faster, however the use of ground control points to scale/geo-reference the models are still required. This often leads to the necessity of using total stations or Global Positioning System (GPS) for the acquisition of ground control points. Although the integrated use of digital photogrammetry and total station/GPS is now common practice, it is clear that this may not always be practical or economically convenient due to the increase in cost of the survey. To address these issues, this research proposes a new method of utilizing photogrammetry for the creation of georeferenced and scaled 3D models not requiring the use of total stations and GPS. The method is based on the use of an object of known geometry located on the outcrop during the survey. Targets located on such objects are used as ground control points and their coordinates are calculated using a simple geological compass and trigonometric formula or CAD 3D software. We present three different levels of survey using (i) a calibrated digital camera, (ii) a non-calibrated digital camera and (iii) two commercial smartphones. The data obtained using the proposed approach and the three levels of survey methods have been validated against a laser scanning (LS) point cloud. Through this validation we highlight the advantages and limitations of the proposed method, suggesting potential applications in engineering geology.

Keywords: digital photogrammetry; low-cost photogrammetry method; characterization of rock slopes; smartphones in photogrammetric analyses

1. Introduction

In the last decade, the use of remote sensing techniques in engineering analyses of slopes has increased dramatically. In particular, laser scanning (LS) and digital photogrammetry (DP) techniques have been described by numerous authors [1–6].

LS is a very powerful survey technique which allows 3D models of slopes to be rapidly produced at high precision and in a small amount of time. Recently the availability of full waveform instruments has made this technique even more attractive, with the possibility of using LS for long range surveys (up

to 6000 m) and displacement monitoring. Furthermore, the availably of aerial platforms, for using this technique, such as helicopter, aircraft and unmanned aerial vehicle (UAV) has allowed the surveying of very high and inaccessible steep slopes at a high resolution. It is however important to note that one of the main limitations of LS remains the high cost of the instrumentation.

DP obtains 3D model of objects by the use of digital cameras. Three main types of acquisition methods can be used: independent convergent, image fan and image strip methods. These methods are explained in detail by Birch [7] and Francioni et al. [8], and their application is discussed by Sturzenegger and Stead [9]. Similar to LS, DP can be acquired from several platforms, such as a helicopter, aircraft and UAV. The advantages and limitations of each platform are discussed by Francioni et al. [8], where it is highlighted that terrestrial hand-held (or tripod-based) DP is the easiest and cheapest method. A limitation associated with this method is the possible presence of occlusions causing holes (zero data) in the point cloud in the case of very high slopes. This limitation can be overcome using helicopters, aerial balloons and UAV platforms, but the cost and the complexity of the survey can increase. In fact, when using a hand-held camera, the cost of DP is very low and mainly related to the resolution and quality of the camera [8].

The recent development of the structure from motion (SfM) method and associated software has made DP significantly easier to use. An introduction to this technique is presented by Westoby et al. [10] while its applications have been recently discussed by Salvini et al. [11], Francioni et al. [12] and Francioni et al. [13]. SfM is based on a highly redundant bundle adjustment matching features in multiple overlapping photographs. Although this technique makes the creation of 3D models easier and faster, the use of ground control points (GCPs) for scaling and georeferencing the models is still required. The acquisition of the GCPs is usually performed using total stations or Global Positioning System (GPS). However, the requirement for such instruments makes the DP surveys more complex and expensive.

The principal objective of this research is to develop a method to create 3D DP georeferenced models without the need for total station/GPS and to highlight the precision and possible applications of the proposed method. Such methodology is based on the use of an object of known geometry as a reference scale; three types of DP surveys are tested using: (i) a calibrated digital camera, (ii) a non-calibrated digital camera and (iii) two commercial smartphones. Types (i) and (ii) are analyzed to show the importance of calibrating the camera for the generation of 3D models while type (iii) is used to investigate the potential use of smartphones to undertake DP.

The surveys were conducted in a travertine slope outcropping on the western side of the town of Civitella del Tronto, Italy (Figure 1A,B). The travertine rock slope is ca 20 m wide and 30 m high and is characterized by two systematic joint sets, J1 and J2, and sub-horizontal bedding planes, S0 [13].

Each of the point clouds obtained by the three DP methods was compared/validated against the LS point cloud and the results were analyzed in terms of areal comparison between 3D point clouds and statistical analyses of 2D profiles. With the goal of understanding the importance of the dimension of an object of known geometry, we have performed different analyses using five and three targets. When using five targets we adopted a 0.5 m × 0.5 m square, while when using three targets they were right-angled and triangular in shape with catheti of 0.5 m the first analysis and 0.25 m in the second.

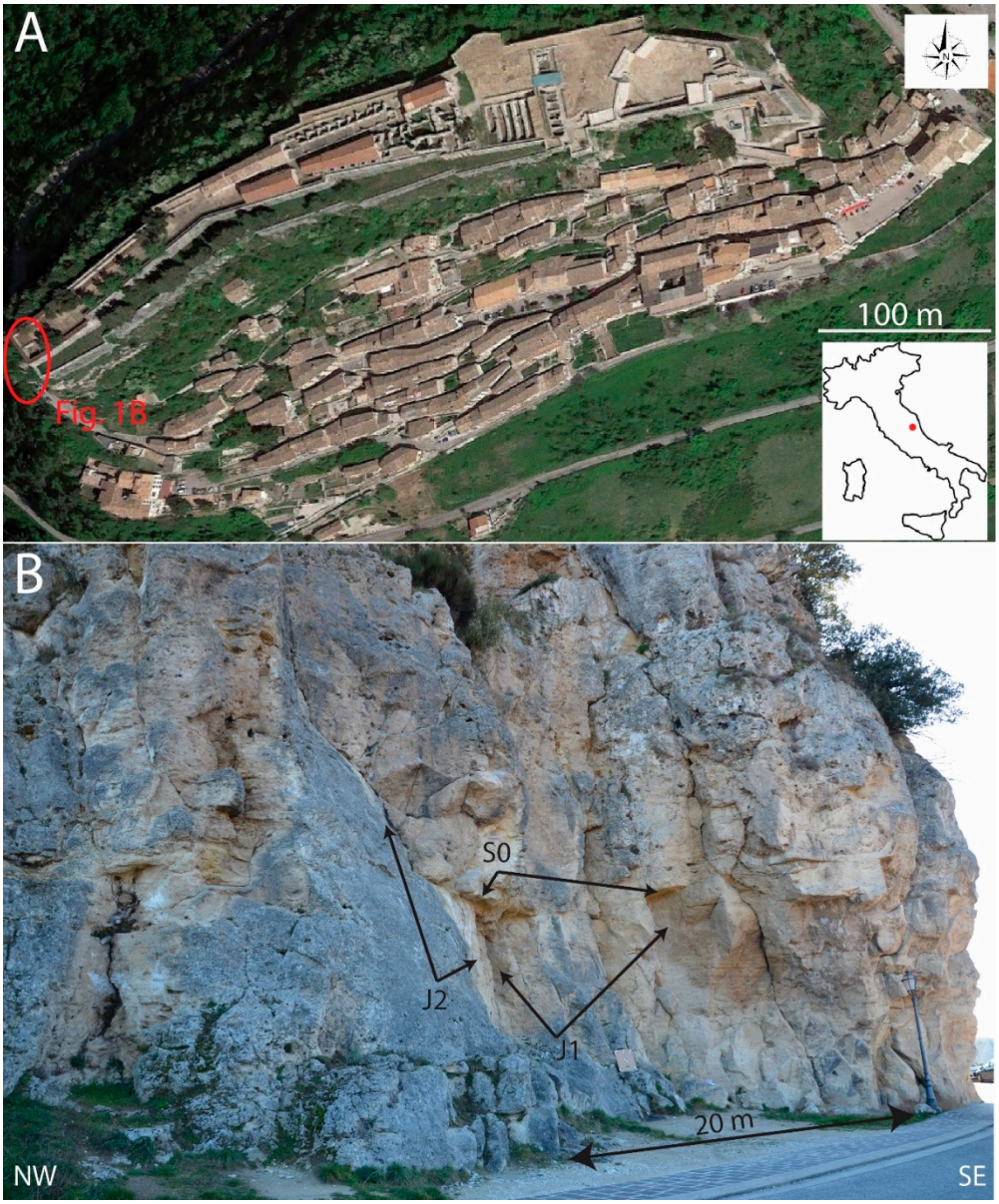

Figure 1. (**A**) Town of Civitella del Tronto, Italy. (**B**) Travertine rock slope outcropping to the west side of the town of Civitella del Tronto. The slope is characterized by two systematic joint sets, J1 and J2, and sub-horizontal bedding planes.

2. Materials and Methods

With the goal of decreasing the costs and the time necessary for the creation of scaled and georeferenced 3D DP models, a new procedure for undertaking DP surveys is described.

2.1. Defining the Coordinate of the Targets

The proposed DP survey method is based on the use of an object of known geometry, located on the slope under study and providing a reference during the creation of the 3D model. The object utilized in this research is a flat wooden square with targets at the four corners, at the mid-point of the upper side and at the center. The wooded square and the distance between each target is shown in Figure 2.

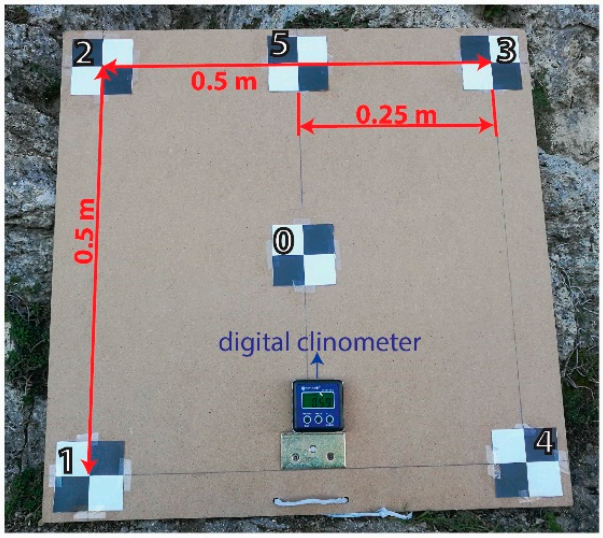

Figure 2. Wooden square and targets used in this study as a reference for the creation of digital photogrammetry (DP) models.

Once the wooden square has been positioned on the slope, a geological compass is used to measure the dip and dip direction of the wooden square surface and the inclination of the the base of the square (this angle can be also measured using a digital clinometer, Figure 2). Using this information, it is possible to reconstruct in 3D CAD software the 3D geometry of the object through four steps, identifying the coordinates of the targets. This procedure is shown in Figure 3, where we have highlighted the adopted procedure step-by-step.

Step 1 - Draw a square representing the geometry of the targets;

using the point 0, 0, 0 as the center of rotation:

Step 2 - incline the square according to the dip measured with the geological compass;

Step 3 - rotate the square by the degree of the dip direction measured with the geological compass;

Step 4 - rotate the base of the square with respect to the angle between the base of the square and the horizontal. This angle can be obtained with a geological compass or with a digital clinometer set up on the square (Figure 2). If the wooden square is located horizontally (angle measured by the clinometer equal to 0) step 4 can be omitted.

The proposed procedure re-creates the geometry of the targets on the wooden square and defines their relative coordinates. These coordinates will be then used as GCPs during subsequent generation of the 3D DP model. It is possible to work in a relative coordinate system based on the origin coordinates 0, 0, 0, or on the global coordinate system by acquiring the GPS position of the target 0, 0, 0.

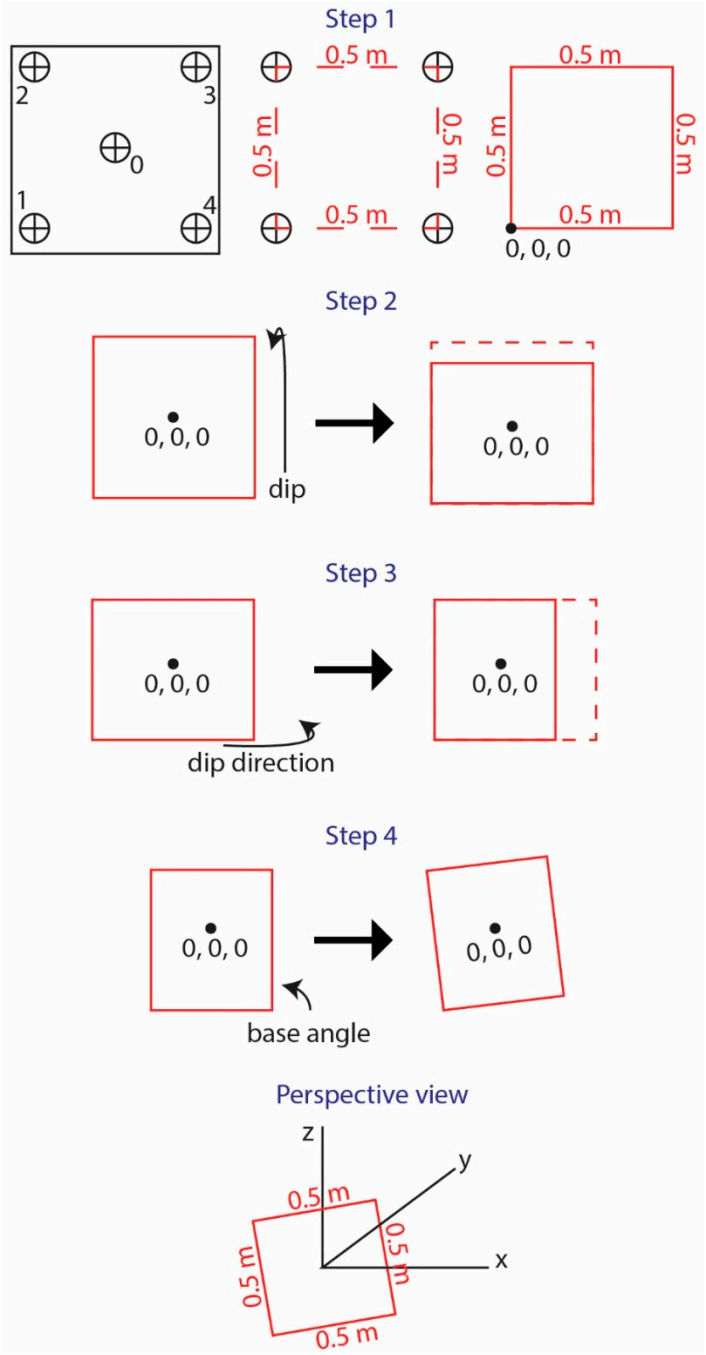

Figure 3. The four steps required to determine the coordinates of the targets using 3D CAD software.

2.2. DP Surveys

2.2.1. DP Surveys with Calibrated and Non-Calibrated Cameras

The camera used for surveys (i) and (ii) was a Nikon D5100 with the following technical specifications: 16.2 million effective pixels, 23.6 mm × 15.6 mm sensor size, 4.78 µm pixel size, and maximum image dimensions of 4928 × 3264 pixels. A f = 18 mm focal length lens was used during the acquisition. Considering this information and the distance between the camera and the object of study, it is possible to calculate the size of the area acquired by each photograph (Figure 4A). In this case, considering imaging of a 23.6 mm width and a focal length of 18 mm, the area acquired by each photograph was ca 6.5 m in width at a distance of 5 m and ca 13 m width at a distance of 10 m (Figure 3B). Considering that the suggested required overlap of photographs for the use of the structure

from motion (SfM) method is ca 80% [14], for a distance between the camera and the object of ca 10 m, the baseline was set at ca 2.6 m (Figure 4B). The survey was conducted using the image fan method [7,8] (Figure 4C); when using such a method, the photographs are captured from specific camera locations (which are not independent). This easily defines, for the DP stations, the area acquired by each photograph and guarantees the correct overlap.

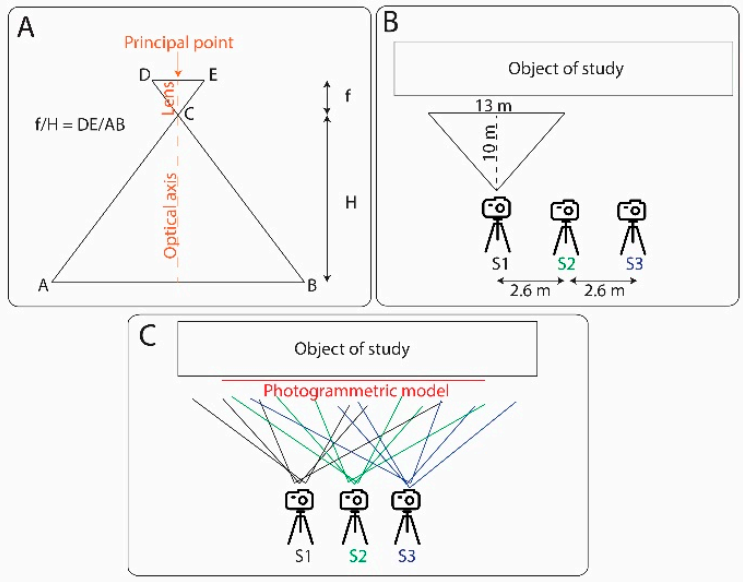

Figure 4. (**A**) Schematic representation of the geometric characteristics of the photographs and associated formula. (**B**) Schematic representation of the DP station and the area of coverage. (**C**) Image fan method.

Camera calibration was undertaken using the software Agisoft Lens [14]. This software allows for visualization of a chessboard on the computer screen. After acquiring at least three photographs of the chessboard from at least three different angles, it is possible to calculate the following camera calibration parameters:

- fx, fy = focal length
- cx, cy = principal point coordinates
- K1, K2, K3, P1, P2 = radial distortion coefficients, using Brown's distortion model

The creation of the DP 3D models has been performed using the software Agisoft PhotoScan [14], a SfM suite for photogrammetric analysis. During the feature matching across the photographs, PhotoScan detects points in the source photographs which are stable under viewpoint and lighting variations and generates a descriptor for each point based on its local neighborhood. These descriptors are then used to detect correspondence across the photographs. The procedure is similar to the well-known SIFT (scale-invariant feature transform) approach, but PhotoScan uses different algorithms for slightly higher alignment quality (PhotoScan, 2018). With regard to the intrinsic and extrinsic camera orientation parameters, PhotoScan uses an algorithm to find approximate camera locations and subsequently refines them using a bundle-adjustment algorithm (PhotoScan, 2018).

2.2.2. DP Surveys with Smartphones

Smartphone 1 has a digital camera with following characteristics: 8 million effective pixels, 4.896 mm × 3.672 mm sensor size, 1.5 µm pixel size, maximum image dimensions of 3264 × 2448 pixels and 29 mm equivalent focal length.

Smartphone 2 uses a digital camera with: 12 million effective pixels, 4.96 mm × 3.72 mm sensor size, 1.25 µm pixel size, maximum image dimensions of 3968 × 2976 pixels and 27 mm equivalent focal length.

With these specifications, the areas acquired by each photograph are ca 17 m and 18 m, respectively, at a distance of 10 m. In light of the suggested required photograph overlap for the use of SfM (ca 80%), when the distance between the smartphone camera and the outcrop was ca 10 m, the baseline was set at ca 3.5 m. The survey was conducted using the image fan method and the model created through PhotoScan.

2.3. LS Surveys

The LS survey was carried using a Leica BLK 360 laser scanner [15] which is able to acquire fully-colored panoramic images overlaid on a high-accuracy point cloud. To obtain high-quality point cloud and textures, multiple LS stations were performed at 3 m and 10 m of distance from the outcrop. In relation to these distances, the resolution was set at 0.03 m and 0.01 m, respectively. The point clouds were fused together and the area covered by the survey was the same as covered by the DP surveys. The LS 3D model was oriented using the same target coordinates utilized for the DP model construction. In this way it was possible to georeference the LS point cloud in the same reference system as the DP model and to compare the models.

3. Results

3.1. Analysis of DP and LS Data Using Wooden Square Targets 1, 2, 3, 4 and 5

The DP and LS surveys were carried out on a travertine rock outcrop (Figure 1B) of ca 20 m width and 30 m elevation. The wooden square was located on the central part of the slope at ca 1 m elevation. When using the digital camera, the survey was conducted at a distance of ca 10 m with a ca 2.6 m long baseline. For each of the five photogrammetric stations used we acquired four photographs of the slope using different lines of sight (image fan method, Figure 4C). Table 1 shows the camera calibration parameters calculated through the camera calibration process while Figure 5 shows the image residuals (distortions) plotted on the image plane.

Table 1. Camera calibration parameters.

Parameter	Value (pixel)	Standard Error
Image width	4928	
Image height	3264	
Principal point (x)	19.9889	0.890748
Principal point (y)	36.4507	0.89439
Radial K1	−0.0628401	0.00235961
Radial K2	0.0652221	0.0132876
Radial K3	−0.105281	0.0295335
Radial K4	0.0729408	0.000503861
Tangential P1	−0.000123014	5.1837e-05
Tangential P2	0.000487723	3.7193e-05

The surveys conducted using a smartphone were undertaken at the same distance from the slope (10 m) with a ca 3.5 m long baseline. Four photogrammetric stations were utilized with three photographs at different lines of sight acquired for each (for a total of 12 photographs).

The LS was set up at the same distance as the DP stations. Table 2 lists the coordinates of each target obtained using the four described steps, while Figure 6A–E show the five 3D models obtained from the calibrated digital camera, the non-calibrated digital camera, smartphones 1 and 2 and a LS. An estimation of the spatial resolution of the point clouds is reported in Table 3.

The four photogrammetric models (Figure 6A–D) were compared with the LS model (Figure 6E) using the software CloudCompare [16]. The results are illustrated in Figure 7, where it is possible to observe the comparison between LS and DP using a calibrated camera (Figure 7A), a non-calibrated digital camera (Figure 7B), smartphone 1 (Figure 7C) and smartphone 2 (Figure 7D). It is apparent that

the differences between the LS and DP models increased in the external part of the slopes (red and blue areas), while they were negligible close to the wooden square. Comparison with the LS indicates that the DP model created using the calibrated and non-calibrated digital cameras was the most precise. Models created with smartphone 1 were more precise than the model created with smartphone 2.

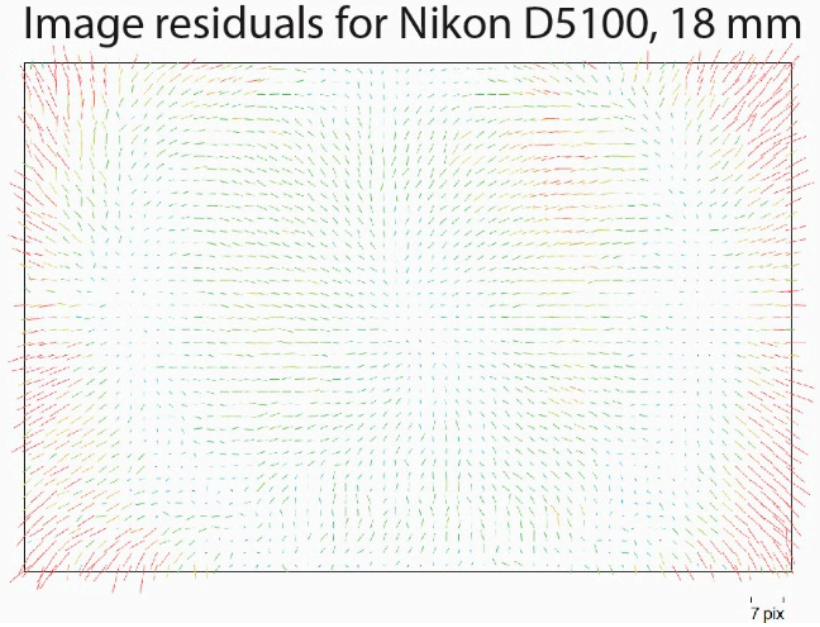

Figure 5. Image residuals (distortions) plotted on an image plane.

Table 2. Target coordinates.

ID	X (m)	Y (m)	Z (m)
0	0	0	0
1	−0.081	0.25	−0.236
2	0.081	0.25	0.236
3	0.081	−0.25	0.236
4	−0.081	−0.25	−0.236
5	0.081	0	0.236

Table 3. Resolution of models using different survey methods.

Type of Survey	Model Resolution (m)
LS	0.003–0.010
DP calibrated camera	0.010
DP non-calibrated camera	0.010
Smartphone 1	0.015
Smartphone 2	0.012

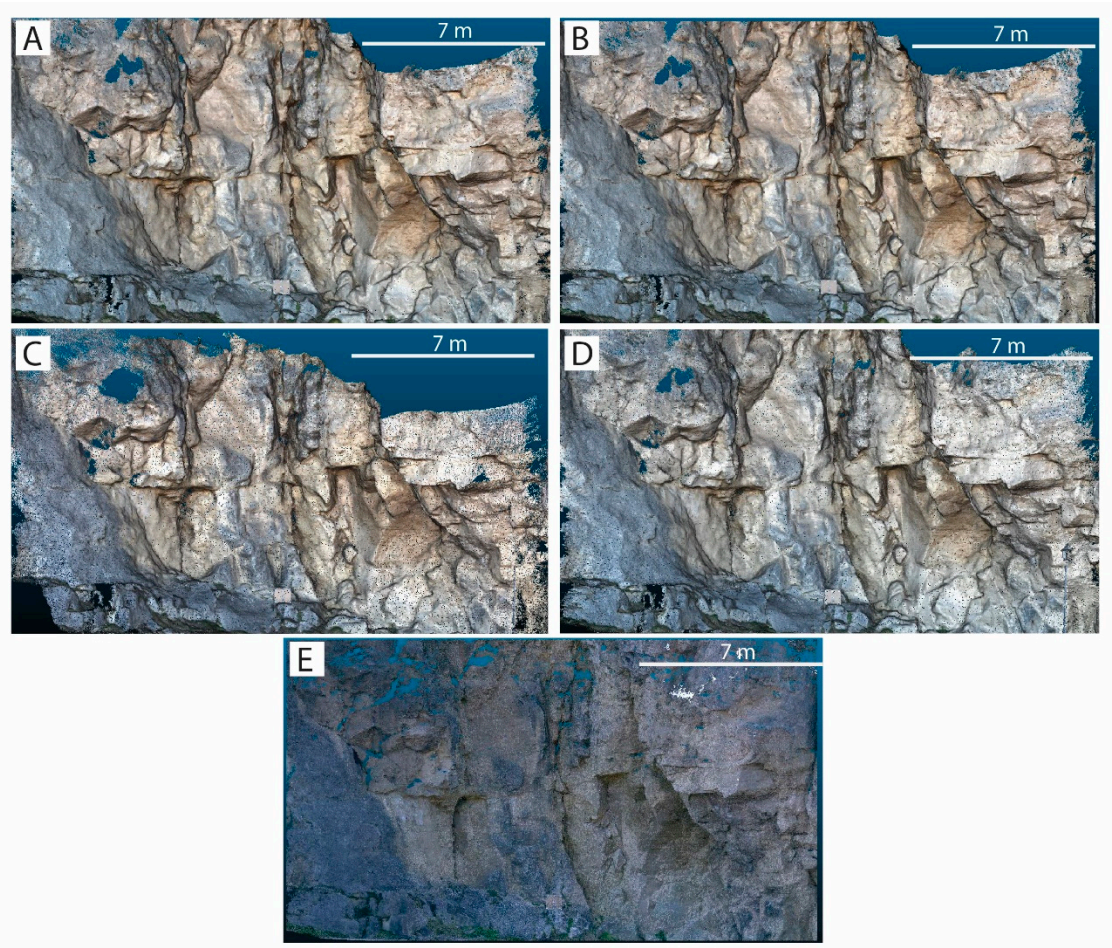

Figure 6. Three-dimensional models obtained using a calibrated digital camera (**A**), non-calibrated digital camera (**B**), smartphone 1 (**C**), smartphone 2 (**D**) and laser scanning (LS) (**E**). View of models towards the east.

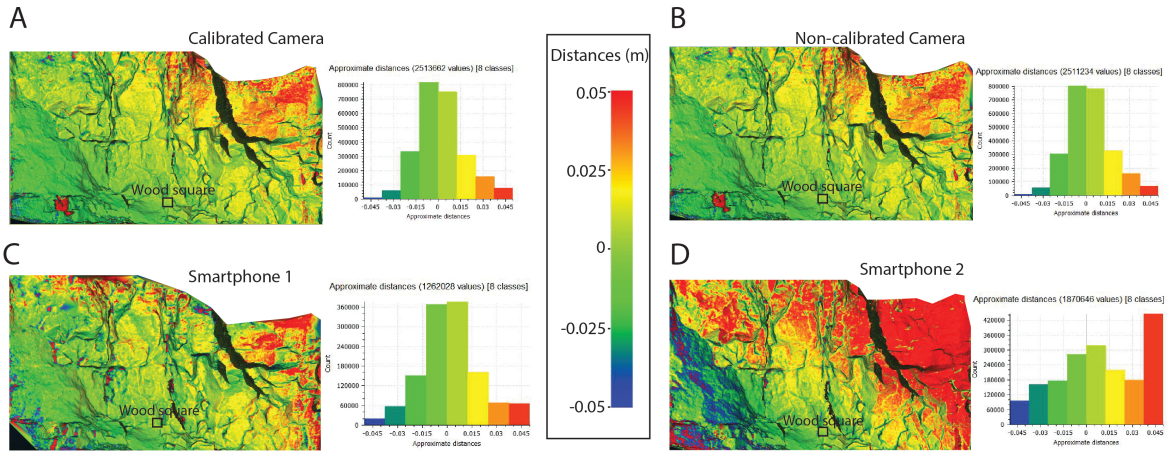

Figure 7. Comparison between LS and DP with calibrated camera (**A**), non-calibrated digital camera (**B**), smartphone 1 (**C**) and smartphone 2 (**D**). Models were georeferenced using the five targets 1–5.

To improve the readability of the results, we used five slope profiles created through each 3D model, starting from the wooden square. Profile 1 is horizontal, and on the left side of the wooden square. Relative to Profile 1, Profiles 2, 3, 4 and 5 are oriented at 45°, 90°, 135° and 180°, respectively. Figure 8 shows the five profiles overlain on the DP model.

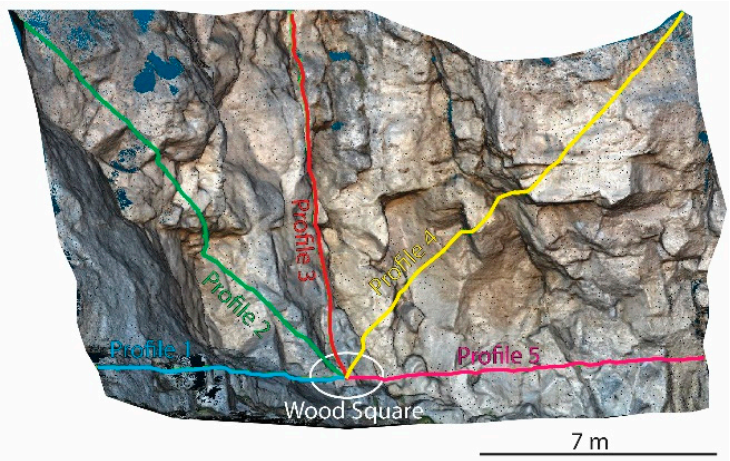

Figure 8. Profiles 1–5 traced on the DP and LS models.

The profiles obtained from the DP models were then compared with the same profiles on the LS model. This was carried out using points extracted from the DP and LS profiles every 0.5 m. The coordinates of every point from the DP profiles were compared with the coordinate of the equivalent point from the LS profile. The results have been plotted graphically in terms of the magnitude of the difference between the same points on the LS and the DP profiles (column chart) and in terms of trendlines. Figure 9 shows the column chart and the trendline for each profile obtained from a comparison between the LS and the calibrated camera, non-calibrated camera, smartphone 1 and smartphone 2 models, respectively.

Black dashed lines in the trendline graphs are located at a distance of 6 m from the wooden square and there is a 0.05 m difference between the LS and DP. In the column charts, 6 m of distance and 0.05 m of difference were highlighted in red. These were included in all the graphs as a reference.

The column chart for the calibrated camera model shows maximum dispersion values up to 0.06 m. Most of the columns lie below 0.05 m and within a 6 m distance from the wooden square, below ca 0.03 m. In the model obtained using the non-calibrated camera, the column chart shows similar results to the calibrated camera although there are more columns above/in proximity of the 0.05 m line (with a few up to 0.16 m). In the model obtained using smartphone 1, the same chart shows several columns above the 0.05 m line and, in general, the dispersion is slightly greater than for the previous models. The column chart for smartphone 2 shows the highest dispersion with several columns above the 0.05 m line.

In general, it appears from the trendline graphs of all the models, that the agreement between the LS and DP models decreases as the distance from the wooden square increases, particularly for the non-calibrated camera and smartphone 2.

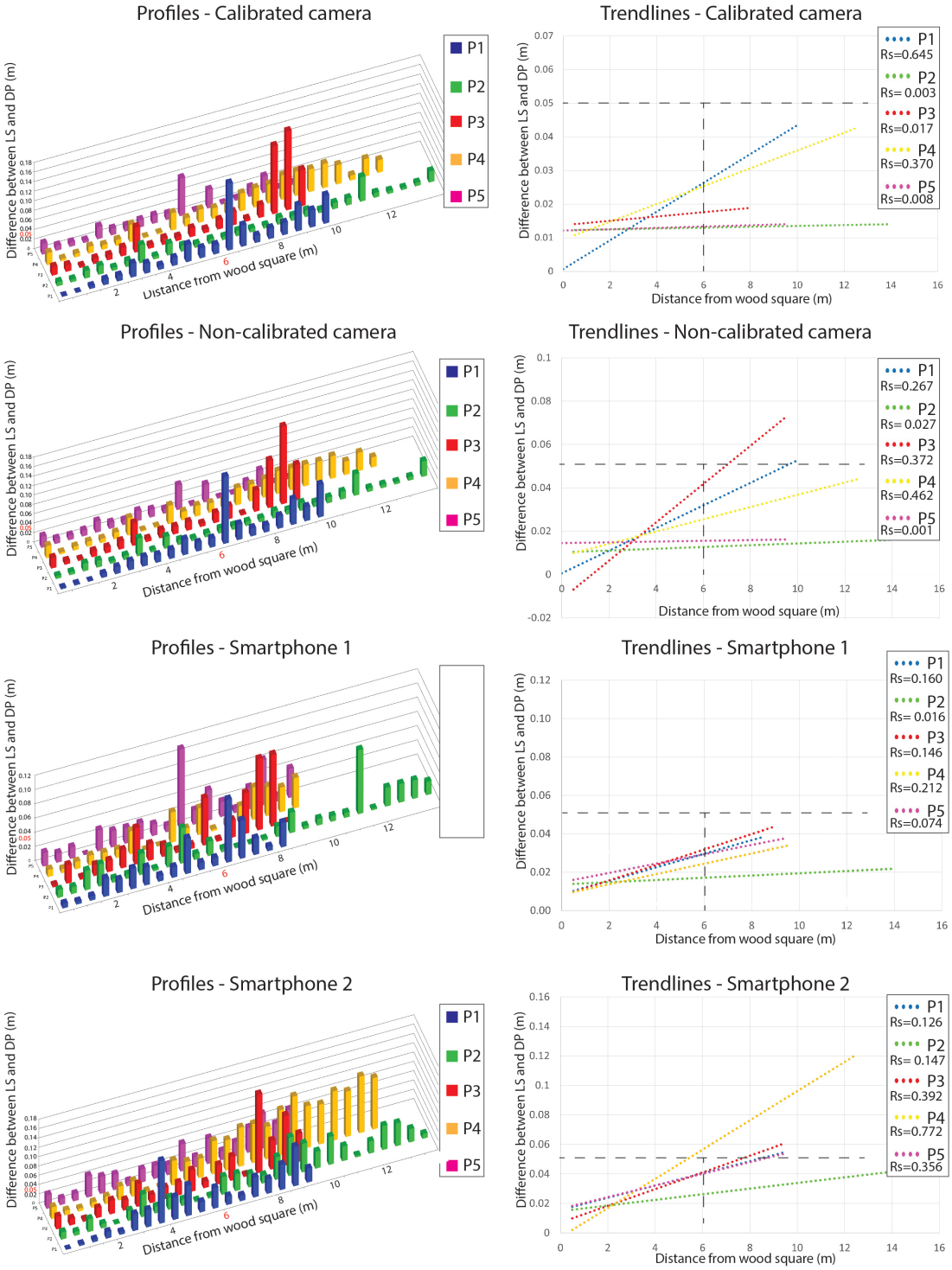

Figure 9. Column charts (left) and trendline graphs (right) obtained from a comparison between the LS and the calibrated camera, non-calibrated camera, smartphone 1 and smartphone 2 models. All models were georeferenced using the five targets 1–5 located on the wooden square. For references, we have included the black dashed lines in the trendline graphs at a distance of 6 m from the wooden square and for indicating a 0.05 m difference between the LS and DP. In the column charts, 6 m of distance and 0.05 m of difference are highlighted in red. Rs in the trendline graphs indicates the R square value.

3.2. Analysis of the DP and LS Data Using the Three Targets 1, 2 and 3

In the previous section, we have shown the results using targets 1–5 on the wooden square. When an object different to the wooden square is used it may be necessary to use less than five targets. To understand the effect of the variation in the number of targets used on the proposed methodology, the DP models have been recreated using three targets 1, 2 and 3 (right-angle triangle with catheti of 0.5 m). The resulting comparison between the DP models obtained and the LS is illustrated in Figure 10A–D. The models from calibrated and non-calibrated digital cameras show similar results; however, the differences seem to be less than obtained using the five targets. In contrast, the differences between the DP and LS results increase using the two smartphones and three targets, especially for the use of smartphone 2.

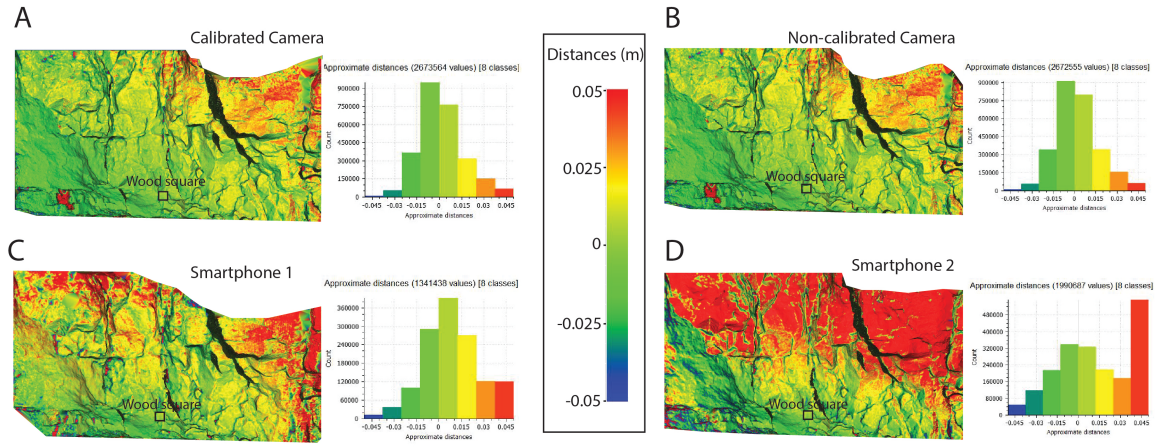

Figure 10. Comparison between LS and DP with a calibrated digital camera (**A**), non-calibrated digital camera (**B**), smartphone 1 (**C**) and smartphone 2 (**D**). All models were georeferenced using the three targets 1, 2, and 3.

Figure 11 shows the dispersion graphs and trendlines obtained from a comparison between the LS and calibrated camera, non-calibrated camera, smartphone 1 and smartphone 2 models, respectively, for the use of three targets, 1, 2 and 3. The column chart for the calibrated digital camera model shows maximum values up to 0.08 m compared to the LS with few points above the 0.05 m line. In general, most of the columns are below the 0.05 m line. In the model obtained from the non-calibrated digital camera, the column chart shows several columns above the 0.05 m line (two up to 0.16 m). As for the calibrated digital camera model, most of the columns lie below the 0.05 line. In the model obtained using smartphone 1, the column chart highlights several columns above the 0.05 m line with numerous columns in the general proximity of this line. The column chart for smartphone 2 shows, as before, the highest dispersion with several columns above the 0.05 m line.

The trendline graphs for all the models show that the agreement between the LS and DP models decreases as the distance from the wooden square increases. As was the case when using five targets, this increase is more evident for the models obtained using the non-calibrated digital camera and smartphone 2.

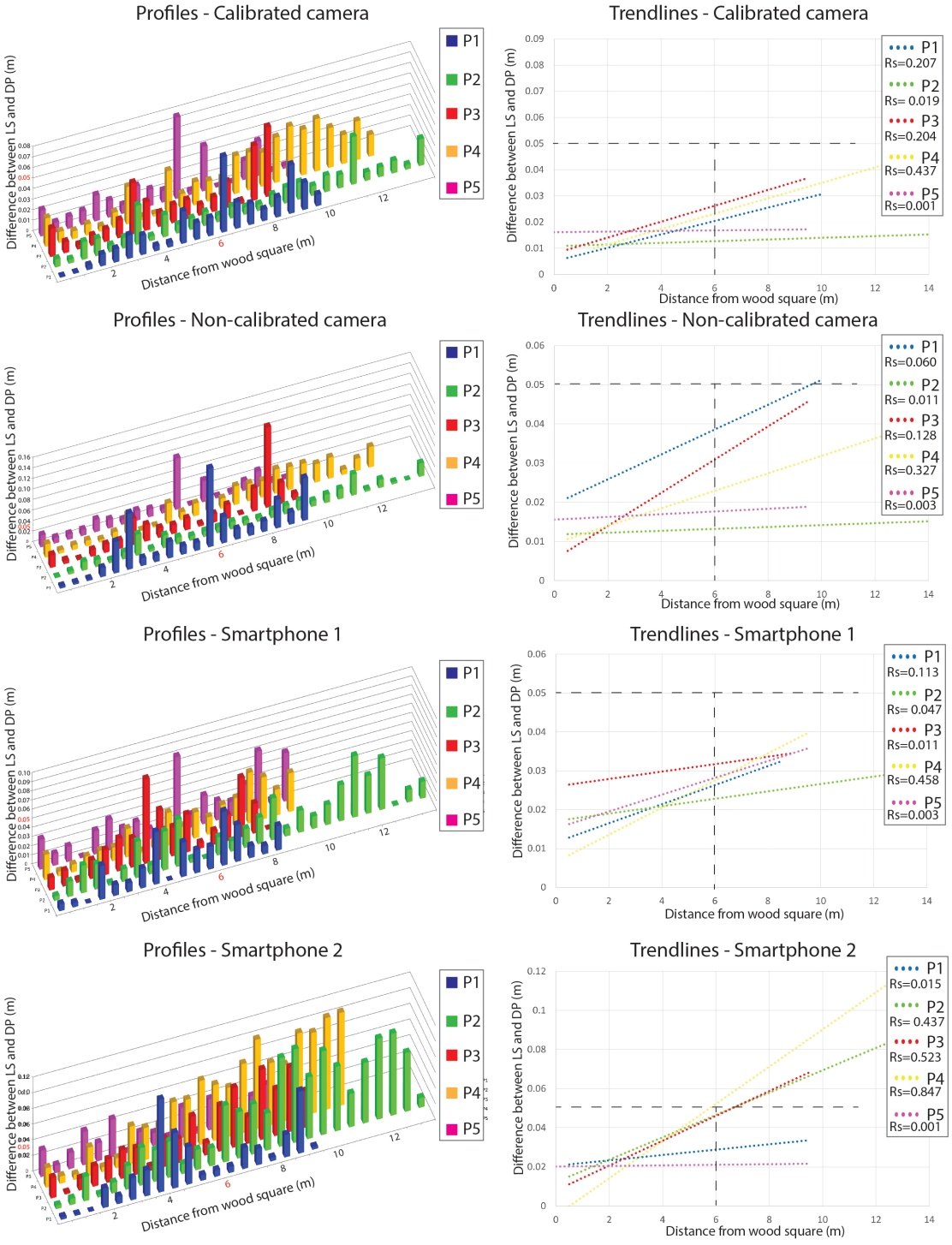

Figure 11. Dispersion graphs (left) and trendline graphs (right) obtained from the comparison between the models from the LS and calibrated camera, non-calibrated camera, smartphone 1 and smartphone 2. All models were georeferenced using the three targets 1, 2, and 3. For references, we have included the black dashed lines in the trendline graphs at a distance of 6 m from the wooden square and for indicating a 0.05 m difference between the LS and DP. In the column charts, 6 m of distance and 0.05 m of difference were highlighted in red. Rs in the trendline graphs indicates the R square value.

3.3. Analysis of the DP and LS Data Using the Three Targets 0, 5, and 3

In order to understand the importance of the dimension of the object used for the georeferencing of the models, we repeated the analysis using the targets 0, 5, and 3 (i.e., for the side of a triangle

0.25 m in width, Figure 2). The results, shown in Figures 12 and 13, highlight that the areas with differences ≥0.005 m increase when compared to the models created using five targets and the targets 1, 2 and 3 (Sections 3.1 and 3.2). Only the model obtained using smartphone 1 appears to not be affected by the use of a smaller dimension reference object. The models obtained using the calibrated and non-calibrated digital cameras produced similar results, with the calibrated camera having lower dispersion (Figure 11E–H).

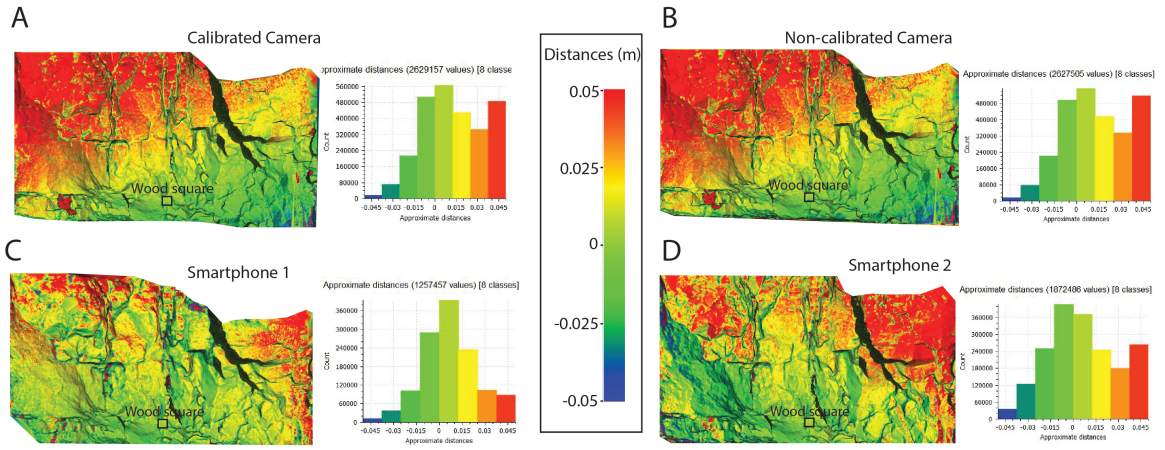

Figure 12. Comparison between LS and DP obtained with a calibrated digital camera (**A**), non-calibrated digital camera (**B**), smartphone 1 (**C**) and smartphone 2 (**D**). All models were georeferenced using the three targets 0, 5, and 3.

Figure 13 shows the column charts and trendlines obtained from a comparison between the LS and calibrated camera, non-calibrated camera, smartphone 1 and smartphone 2 models, respectively. The column charts show that the model obtained using the calibrated digital camera has a maximum dispersion value of up to 0.24 m with few columns between 0.1 and 0.15 m. Most of the columns, however, lie below or in proximity of the 0.05 m line. In the model obtained using the non-calibrated digital camera, the column chart shows results similar to the calibrated digital camera, but with more columns above/in proximity of the 0.05 m line (with a few up to 0.1 m). In the model obtained using smartphone 1, the chart shows several columns above the 0.05 m line with most of the columns generally in proximity of the 0.05 m line. The results for smartphone 2 are similar to that for smartphone 1, with several columns lying above the 0.05 m line, but with most columns generally in proximity to the 0.05 m line.

As for the models obtained using the three targets, 1, 2 and 3, the trendline graphs for all the DP models show that the agreement with the LS models decreases as the distance from the wooden square increases. The models obtained with smartphone 1 are the least influenced by the distance from the wooden square although the differences highlighted by the dispersion graphs are higher when compared to the calibrated and non-calibrated digital cameras.

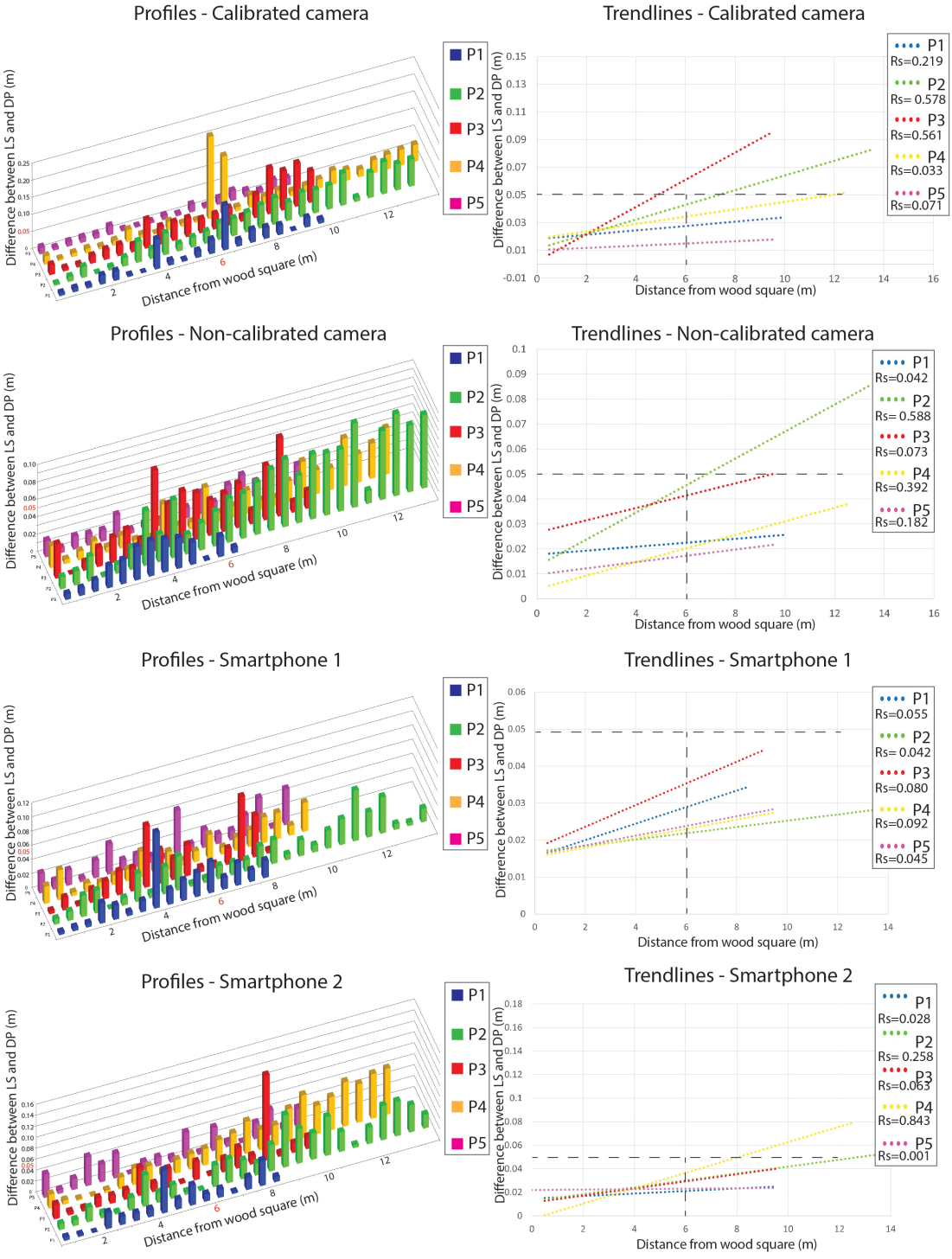

Figure 13. Dispersion graphs (left) and trendline graphs (right) obtained from comparison between the LS models and the calibrated camera, non-calibrated digital camera, smartphone 1 and smartphone 2 models. All models were georeferenced using the three targets 0, 5, and 3. For reference, we have included the black dashed lines in the trendline graphs at a distance of 6 m from the wooden square and for indicating a 0.05 m difference between the LS and DP. In the column charts, 6 m of distance and 0.05 m of difference were highlighted in red. Rs in the trendline graphs indicates the R square value.

3.4. Potential Engineering Geological Data Derived from DP Models

The proposed approach easily obtains oriented and scaled 3D models of rock slopes. Such 3D models can be used to define engineering geological parameters useful for the geomechanical

characterization of the rock slope under study. The software used for this purpose is the freeware code CloudCompare [16]. The first step to be undertaken in rock slope characterization is to define the orientation of the slope and fully exposed planar discontinuities. In CloudCompare, a plane is fitted to selected points on a surface (using least squares), providing an estimate of the discontinuity orientation (dip/dip direction).

The quality of such measurements is related to the quality of the 3D model as presented in Section 3.1, and the precision of the georeferencing. To further verify the quality of the DP models and their orientation, and understand how the differences in the point cloud quality can affect the final results in terms of discontinuity characterization, we have compared measurements of the same discontinuity surfaces taken from the DP and LS models (Figure 14A–D) and in the field with a geological compass. The results of this comparison are shown in Figure 14 and clearly highlight good agreement between the manual and DP/LS measurements.

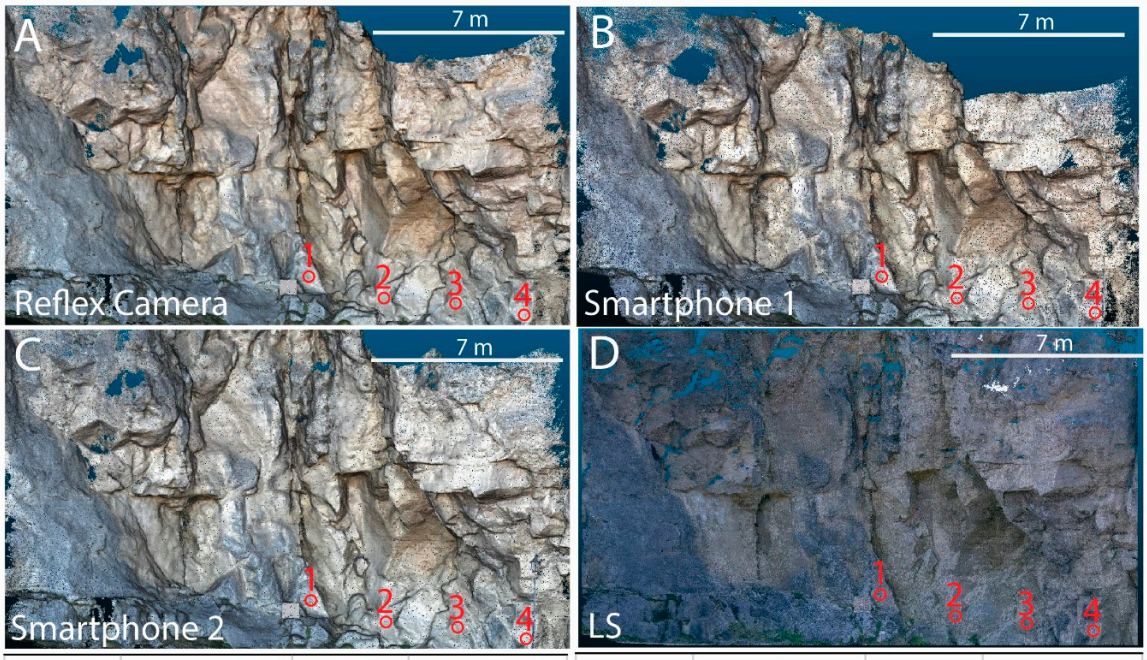

	Method	Dip	Dip direction
Surface 1	Compass	86	247
	Reflex	87	248
	Smartphone 1	89	248
	Smartphone 2	88	248
	LS	89	250

	Method	Dip	Dip direction
Surface 2	Compass	72	114
	Reflex	71	113
	Smartphone 1	72	114
	Smartphone 2	77	114
	LS	67	112

	Method	Dip	Dip direction
Surface 3	Compass	82	298
	Reflex	88	295
	Smartphone 1	88	297
	Smartphone 2	88	296
	LS	87	297

	Method	Dip	Dip direction
Surface 4	Compass	74	276
	Reflex	77	271
	Smartphone 1	79	277
	Smartphone 2	79	272
	LS	79	275

Figure 14. Comparison of dip and dip direction of the discontinuity surfaces measured with a geological compass and from the DP (**A, B** and **C**) and LS (**D**) models. Calibrated and non-calibrated digital camera models are reported as "reflex" (**A**) since they show similar results.

CloudCompare offers the ability to manually extract the discontinuity dip and dip direction (selecting the feature we want to measure as shown in Figure 14) or automatically, using the facet

plug-in [17]. The facet plug-in automatically extracts planar facets (e.g., fracture planes) from point clouds and classifies them based on their orientation and their (orthogonal) distance, displaying the orientations on a stereogram/stereoplot [17]. Figure 15 shows an example of manual (Figure 15A) and automatic (Figure 15B) feature extraction in CloudCompare with the stereonet representation of the 3D DP models.

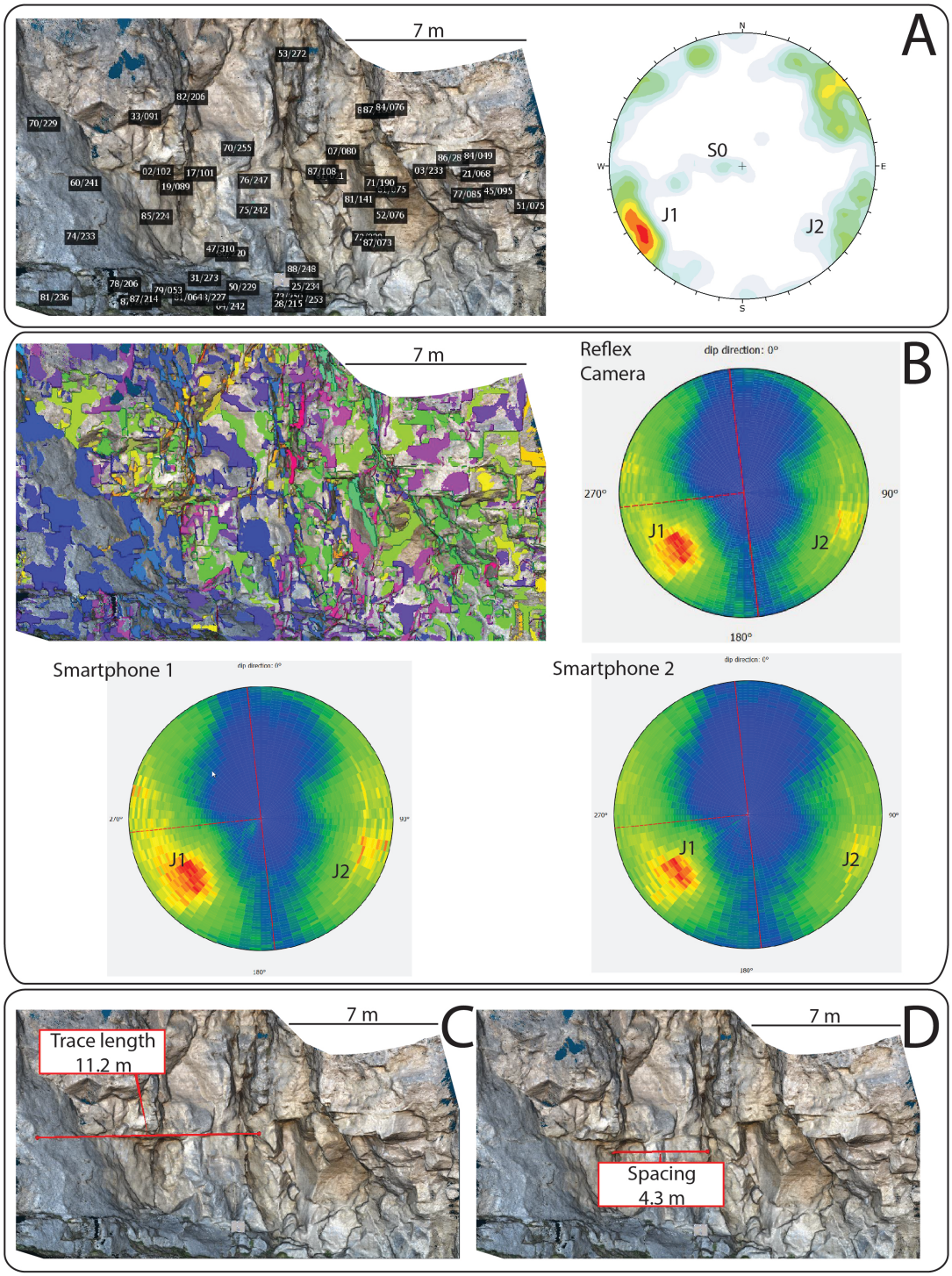

Figure 15. (**A**) Manual extraction of discontinuity orientations and related stereonet. (**B**) Example of automatic extraction of discontinuity orientations and stereonets of DP models using the facet plug-in; calibrated and non-calibrated digital camera models are reported as "reflex" since they show similar results. (**C**) Definition of discontinuity trace length. (**D**) Definition of discontinuity spacing.

Once the main discontinuity sets are obtained, it is important to define their spacing and trace length. This can be achieved by measuring the distance between two points representing these parameters. Figure 15 C–D highlights an example of this procedure.

Using these parameters, it is possible to calculate geomechanical parameters such as the joint volumetric count (Jv = Σ 1/S1 + 1/S2 + 1/S3) and the rock quality designation (RQD). Furthermore, using sampling windows of known geometry, the Joint intensity (Ji) expressed as the length of joints per unit area (L-1) [18] can be extracted [9,13].

By integrating the geometry of the main discontinuity sets with slope attitude, which can be calculated by fitting the plane to the slope (Figure 16), it is possible to perform kinematic stability analyses and verify the possible/probable slope failure mechanisms.

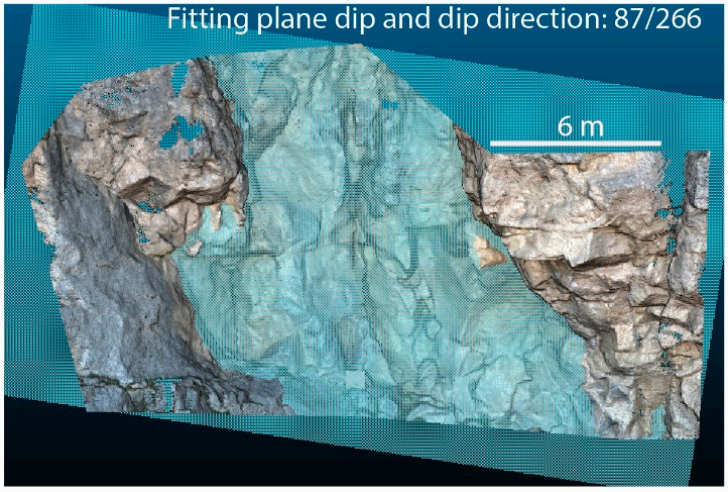

Figure 16. Extraction of slope orientation in CloudCompare.

Finally, another important parameter that can be obtained from the point cloud is the joint roughness. Joint roughness is usually measured using a joint profiling comb placed along a ca 0.01 m discontinuity section. To undertake joint roughness measurement, the point cloud should have a sufficiently high resolution, which may require a 3D model specifically for roughness measurement. Figure 17 shows an example of joint roughness extracted from a high-resolution DP discontinuity surface model (Figure 17A), and comparison with the profile obtained using the joint-profiling comb (Figure 17B).

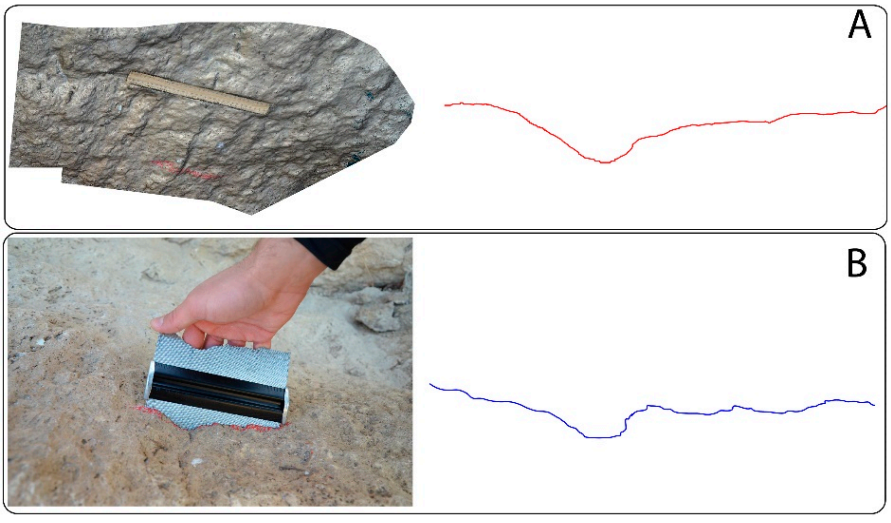

Figure 17. Joint roughness extracted from a high-resolution DP model (**A**) and joint-profiling comb (**B**).

4. Discussion

The use of DP has been widely documented in recent decades. In this research, we proposed a new approach which aimed to substantially reduce the cost and time associated with the use of DP in the analysis of rock slopes. DP, without doubt, represents one of the most cost-effective survey techniques used in many branches of the geosciences [8]. However, in engineering geological studies, the DP 3D model has to be georeferenced in order to extract feature dimensions and the dip and dip direction of geological features. The need to georeference models usually requires the use of total station or GPS, increasing both the complexity and the cost of the work. Francioni et al. [19] previously highlighted the importance of using the TS in georeferencing LS and DP models.

The method proposed in this research is based on the use of an object of known geometry. The 3D DP models obtained from this approach have been compared with LS point clouds and the results analyzed in terms of areal comparison between the 3D point clouds and statistical analyses of 2D profiles. The statistical 2D analysis was carried graphically using column charts to highlight the magnitude of the difference between the same points on the LS and the DP profiles, and in terms of trendlines. Due to the high variability of the data plotted in the trendline graphs, documented by the low Rs values, the trendlines have only been used to verify the general trend of the profile differences. The results show that the proposed methodology allows the creation of a georeferenced 3D model of rock slopes without the use of TS/GPS. The differences between the DP and LS models are associated with the distance from the object of known geometry and type of camera used during the survey, being more precise when using digital reflex calibrated cameras and with only a slight decrease in precision compared to LS when using non-calibrated digital cameras and smartphone cameras. In general, it is apparent that the difference in data quality between the use of a calibrated and non-calibrated digital camera is minimal. The differences in results using DP models obtained with smartphones is highly influenced by the type of smartphone camera used, being in this research less precise when using smartphone 2. Although smartphones can provide useful rock slope data, it is important to consider the choice of the smartphone carefully.

The dimension of the object of known geometry plays an important role in the final precision of the model. In fact, when using an object of small dimensions (0.25 m side triangle), the precision of the models decreases, particularly when using reflex digital cameras.

The number of targets used in georeferencing the models appears to be of minor importance, with similar results achieved using the three targets 1–3 (0.5 m side triangle) and the five targets 1–5 (0.5 m side square). However, this result is strongly related to the fact that the targets used in this research are very close to each other (on the wooden square) and that the outcrop is small. When using typical DP techniques, the GCPs should be spread out as much as possible on the study area, and the numbers decided according to the dimension of the outcrop [20].

The precision of the georeferencing is related to the metric quality of the targets and the precision of the measurements obtained from the geological compass for the orientation of the object of known geometry. In this research, we have used black and white, 8-cm-wide targets. Considering that the survey was conducted at a distance of 10 m from the outcrop, the targets were easily recognizable during the creation/orientation of the DP 3D model. This obtained, during the assignation of target coordinates, errors lower than 1 mm. With regard to the precision of the measurements obtained from a geological compass, Novakova and Pavlis [21] measured the same fracture with an analogue compass more than a hundred times, obtaining a standard deviation for dip direction of all measurements of 1.34°, and 0.93° for the dip. The maximum difference among the measurements was 5°. In light of this study, the dip and dip direction of the object of known geometry were measured several times to decrease the errors associated with the precision of the geological compass (Novakova and Pavlis [21]).

Furthermore, it is important to note that the quality of the DP 3D model is connected to the quality of the photographs acquired during the survey. In this case, the slope was easily accessible and the lighting conditions optimal and, consequently, it was possible to create high-quality DP models. In the case of unfavorable lighting conditions or very complex slope geometry, the quality of the DP models can decrease.

The engineering rock mass parameters extracted from the DP point clouds, using the proposed methods, can be considered reliable and have been shown to be in good agreement with measurements taken in the field. The measurements of dip and dip direction of discontinuities show only a few degrees of variation, which is within the range of conventional geological compass errors. Discontinuity surfaces can be extracted manually or automatically. However, although algorithms for automatic features extraction are very useful and permit a remarkable number of features in a very short time, the control on such features is minimal and it is often difficult to be confident whether the extracted features are natural discontinuities, excavation surfaces or artifacts. An example of this is shown in Figure 15, where the manual and automatic extraction of geological features is highlighted. Although it is possible to see a good agreement between manually and automatically extracted features associated to J1 and J2, the absence of the less visible S0 on the stereonet, based on the automated extraction algorithm, is apparent. The automatic feature extraction has been carried out in the DP models from the reflex digital camera and smartphones. The stereonets obtained from this procedure show similar results in the three cases, highlighting that the lower precision obtained in the DP models using smartphones does not affect automatic discontinuity extraction results.

Joint trace length and spacing can be easily determined from the point cloud by measuring the exposed trace length of a joint and the distance between individual joints within a joint set, respectively. Joint roughness can be extracted by creating profiles along the discontinuity surface. In this case, if the point cloud does not have a sufficiently high resolution, it may require a 3D model specifically obtained for roughness measurement. Similar approaches for the extraction of joint roughness from DP and/or LS have been documented by Haneberg [22], Poropat [23] and Kim et al. [24].

In light of these considerations, the proposed DP approach can be highly suited to acquiring rock mass parameters (slope and discontinuity attitude, discontinuity spacing and persistence, joint roughness, etc.). However, in relation to the errors highlighted by the different DP acquired models when compared to the LS data, it has to be noted that this methodology is not suited for analyses requiring higher accuracy such as slope monitoring or multi-temporal change detection analyses [25,26].

The uses of an object of known geometry represents a limitation when dealing with wide or high elevation rock slopes. In fact, we have shown that the errors increase with increasing the distance from the reference object. Therefore, we suggest that the proposed method is highly suited and reliable for 3D models of width less than ca 25–30 m, when the object is located at the center of the outcrop. When the object cannot be located at the center, according with the differences highlighted by the column charts, the data can be considered reliable within a ratio of ca 10–15 m from the object. For rock slope DP models of width 25–30 m or greater, the use of the proposed method would require larger dimension objects than used in this research. Further research and calibration would also be required to ensure the errors in use of an extension to the proposed to large outcrops method are acceptable. A practical option to overcome the above limitation is to move the object laterally along the slope after the DP survey, and perform a window mapping survey. With this approach, it is possible to create several subsequent DP 3D models of width less than ca 25–30 m. Each model will be oriented through the approach shown in this research. The use of window mapping surveys using DP data has been shown, among others, by Sturzenegger and Stead [9] and Francioni et al. [9].

In this research we used a wooden square as the object of known geometry. However, any type of object can be utilized using the same procedure reported in this research. An example is shown in Figure 18 where two 3D models have been created using an emergency warning triangle (Figure 18A) and a ruler-angle measurement instrument (Figure 18B). As before, when using this object, we have to take into account the dimension of the object and always confirm the reliability of the models with manual measurements taken in the field. The use of such highly portable objects allows the proposed method to also be used in remote and difficult to access areas.

With regard to the cost and time associated with rock slope characterization, the proposed approach significantly decreases the cost of the survey. In fact, the possibility of creating a 3D georeferenced model of a slope without the use of a TS and/or GPS, limits the cost incurred to the use of a digital

camera or smartphone. Furthermore, the survey in this way becomes easier to undertake and, more importantly, faster, reducing the risk for the mapping personnel. Regarding the post-processing of photographs, the costs are similar to conventional photogrammetric techniques, with the ability to use open source software (e.g., VisualSFM [27] for structure from motion and CloudCompare for managing the point clouds), in addition to proprietary software, such as Agisoft Photoscan.

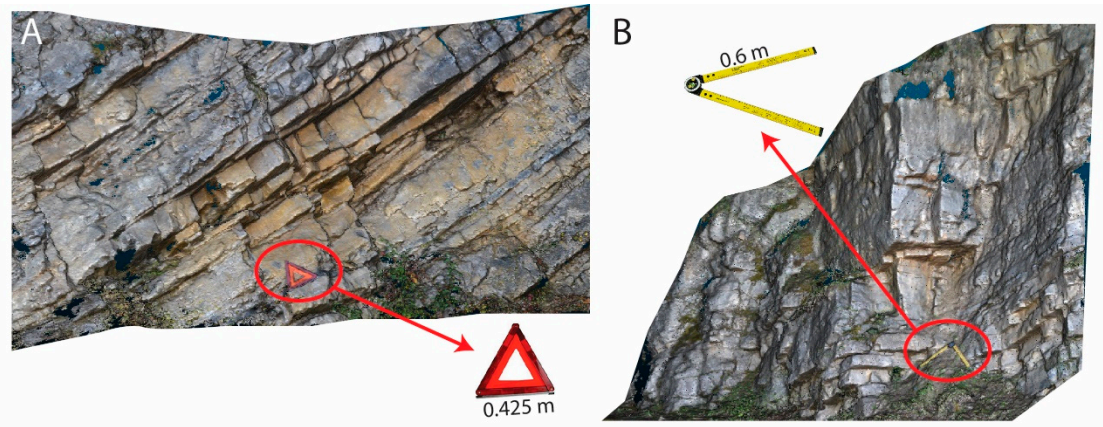

Figure 18. Three-dimensional models created using an emergency warning triangle (**A**) and a ruler-angle measure (**B**).

The use of a smartphone as presented allows a further decrease in the cost and the complexity of the survey. Novakova and Pavlis [21] assessed the precision of smartphones and tablets for the measurement of planar surface orientations, highlighting the good agreement between smartphone/tablet data and geological compass measurements. However, the use of such devices in the DP analysis of rock slopes has not previously been documented in literature and can represent an important tool for the geomechanical characterization of rock masses in a fast and safe way. The results presented show that although the smartphone can provide useful data for DP and rock slope measurements, the type of smartphone camera used significantly influences the results obtained. For this reason, it is essential to verify the data, comparing/constraining these with manual measurements in the field.

Table 4 highlights the advantages and limitations of the different hand-held DP techniques in relation to the results obtained in this study.

Table 4. Advantages and limitations of the different hand-held DP techniques.

DP Technique	Advantages	Limitation
DP with hand-held reflex camera and TS or GPS	Full control of the camera. Photographs can be acquired with great precision without problems associated with lateral extent of the outcrop. Total stationallows to acquire GCPs on the entire outcrop surface. The DP model created using TS GCP will be very accurate. Data extracted can be used for engineering geological interpretation and data extraction.	Cost of the instrumentation includes both the digital camera and TS/GPS. Presence of occlusions in the case of very high slopes. Difficult/impossible to use in poorly accessible areas.
DP with hand-held reflex camera and object of known geometry	Full control of the camera. Photographs can be acquired with great precision. High portability of the instrumentation. Limits the cost incurred to the use of a digital camera. Reduces the time of the survey and therefore decreases the risk to the surveyor. Data extracted can be used for engineering geological interpretation and post processing.	Cost of the instrumentation limited to the digital camera. Presence of occlusions in the case of very high slopes. The precision of the DP models is more influenced by the object used for georeferencing and decreases toward the outer limits of the derived models.
DP with smartphones and object of known geometry	Precision of photographs is limited according to the smartphone used. Very high portability of the instrumentation and cost-free. Reduces the time of the survey and therefore decreases the risk to the surveyor. Data extracted can be used for engineering geological interpretation and post processing.	Presence of occlusions in the case of very high slopes. The precision of the DP models is more highly influenced by the object used for georeferencing and decreases toward the outer extent of the derived models. The precision is also strongly influenced by the type of smartphone camera used. Therefore, when using the smartphone to obtain DP it is highly recommended to always validate the data against field measurements.

5. Conclusions

A new method to create scaled and georeferenced DP models is presented. The procedure proposed is based on the use of an object of known geometry. The proposed method has been rigorously validated against LS data and showed a close agreement between the LS and DP data measurements. The precision of the DP models is influenced by the object used for georeferencing and decreases in the outer extent-derived models. Of the cameras tested, the best results are obtained with the reflex digital camera. The difference however between the use of a reflex calibrated digital camera and non-calibrated digital camera is minimal; the calibrated digital camera shows only minor errors compared to the LS data.

Smartphones can, if needed, be used to replace reflex digital camera in rock slope mapping but it is important to note that the precision of the DP model decreases, as would be expected, compared to digital cameras and it is strongly influenced by the type of smartphone camera used. Therefore, when using the smartphone to obtain DP it is highly recommended to always validate the data against field measurements.

The dimension of the object of known geometry used to georeference the DP plays an important role. Dispersion from LS data when using reflex cameras and a 0.5 m × 0.5 m square, or a 0.5 m side length triangle, was ca 0.03 at 6 m from the wooden square and usually within 0.05 at a distance of 14 m. Therefore, when using objects of similar dimension as the one used in this research, the outcrop should be at most 25–30 wide. If the object is smaller, such as the 0.25 m side triangle (shown when using targets 0, 5, and 3), the errors increase and, therefore, small reference objects should only be used for small outcrops, up to 5–10 m. This limitation can however be easily overcome in practice by moving the object laterally and adopting a window mapping approach.

The comparison of measurements on discontinuity surfaces from the DP models, and in the field using a geological compass, together with the extraction of discontinuity data such as spacing, persistence and roughness, clearly highlight that the proposed DP technique is suitable for engineering geological mapping such as engineering rock mass characterization.

The costs associated with this method are minimal and relate only to the camera cost itself. When using a smartphone, the survey can generally be considered cost-free. Furthermore, the proposed procedure reduces the time of the survey and therefore decreases the risk to the surveyor.

Author Contributions: Conceptualization, M.F., D.S., F.C.; methodology, M.F.; software, M.F. and M.S.; validation, M.F., M.S., G.M.; formal analysis, M.F., M.S., G.M.; investigation, M.F. and M.S.; resources, N.S. and F.C.; data curation, M.F., M.S., D.S. and N.S.; writing—original draft preparation, M.F.; writing—review and editing, D.S. and F.C.; visualization, M.F.; supervision, D.S., N.S. and F.C.; project administration, F.C. and N.S.; funding acquisition, F.C.

Funding: This research was funded by MIUR ex-60% grant awarded to F. Calamita.

Acknowledgments: The authors wish to thank Raffaele Di Ceglie (University BG. d'Annunzioˆ of Chieti-Pescara, Chieti, Italy) for his support during the engineering geological survey. Moreover, we would like to express our gratitude to the reviewers, who provided important and constructive suggestions for improving the quality of the paper.

Conflicts of Interest: The authors declare no conflicts of interest.

References

1. Salvini, R.; Francioni, M.; Riccucci, S.; Bonciani, F.; Callegari, I. Photogrammetry and laser scanning for analyzing slope stability and rock fall runout along the Domodossola? Iselle railway, the Italian Alps. *Geomorphology* **2013**, *185*, 110–122. [CrossRef]
2. Francioni, M.; Salvini, R.; Stead, D.; Giovannini, R.; Riccucci, S.; Vanneschi, C.; Gulli, D. An integrated remote sensing-GIS approach for the analysis of an open pit in the Carrara marble district, Italy: Slope stability assessment through kinematic and numerical methods. *Comput. Geotech.* **2015**, *67*, 46–63. [CrossRef]

3. Spreafico, M.C.; Cervi, F.; Francioni, M.; Stead, D.; Borgatti, L. An investigation into the development of toppling at the edge of fractured rock plateaux using a numerical modelling approach. *Geomorphology* **2017**, *288*, 83–98. [CrossRef]
4. Wolter, A.; Stead, D.; Ward, B.C.; Clague, J.J.; Ghirotti, M. Engineering geomorphological characterisation of the Vajont Slide, Italy, and a new interpretation of the chronology and evolution of the landslide. *Landslides* **2016**, *5*, 1067–1081. [CrossRef]
5. Donati, D.; Stead, D.; Ghirotti, M.; Brideau, M.-A. A model-oriented, remote sensing approach for the derivation of numerical modelling input data: Insights from the Hope Slide, Canada. In Proceedings of the ISRM International Symposium 'Rock Mechanics for Africa' AfriRock Conference, Cape Town, South Africa, 3–5 October 2017.
6. Mazzanti, P.; Schilirò, L.; Martino, S.; Antonielli, B.; Brizi, E.; Brunetti, A.; Margottini, C.; Mugnozza, G.S. The contribution of terrestrial laser scanning to the analysis of cliff slope stability in Sugano (Central Italy). *Remote Sens.* **2018**, *10*, 1475. [CrossRef]
7. Birch, J.S. Using 3DM Analyst mine mapping suite for rock face characterization. In *Laser and Photogrammetric Methods for Rock Face Characterization*; Tonon, F., Kottenstette, J., Eds.; ARMA: Golden, CO, USA, 2006; pp. 13–32.
8. Francioni, M.; Salvini, R.; Stead, D.; Coggan, J.J. Improvements in the integration of remote sensing and rock slope modelling. *Nat. Hazards* **2018**, *90*, 975–1004. [CrossRef]
9. Sturzenegger, M.; Stead, D. Close-range terrestrial digital photogrammetry and terrestrial laser scanning for discontinuity characterization on rock cuts. *Eng. Geol.* **2009**, *106*, 163–182. [CrossRef]
10. Westoby, M.J.; Brasington, J.; Glasser, N.F.; Hambrey, M.J.; Reynolds, J.M. 'Structure-from-Motion' photogrammetry: A low-cost, effective tool for geoscience applications. *Geomorphology* **2012**, *179*, 300–314. [CrossRef]
11. Salvini, R.; Riccucci, S.; Gullì, D.; Giovannini, R.; Vanneschi, C.; Francioni, M. Geological application of UAV photogrammetry and terrestrial laser scanning in marble quarrying (Apuan Alps, Italy). *Eng. Geol. Soc. Territ.* **2015**, *5*, 979–983.
12. Francioni, M.; Coggan, J.; Eyre, M.; Stead, D. A combined field/remote sensing approach for characterizing landslide risk in coastal areas. *Int. J. Appl. Earth Obs. Geoinf.* **2018**, *67*, 79–95. [CrossRef]
13. Francioni, M.; Stead, D.; Sciarra, N.; Calamita, F. A new approach for defining Slope Mass Rating in heterogeneous sedimentary rocks using a combined remote sensing GIS approach. *Bull. Eng. Geol. Environ.* **2019**, in press. [CrossRef]
14. Agisoft. Agisoft Photoscan (version 1.4) 2018. Available online: http://www.agisoft.com/ (accessed on 2 July 2018).
15. Leica-geosystems. 2019. Available online: https://leica-geosystems.com/products/laser-scanners/scanners/blk360 (accessed on 7 January 2019).
16. CloudCompare V.2.9, GPL Software 2018. Available online: http://www.cloudcompare.org/ (accessed on 2 July 2018).
17. Dewez, T.J.B.; Girardeau-Montaut, D.; Allanic, C.; Rohmer, J. Facets: A Cloudcompare Plugin to Extract Geological Planes from Unstructured 3D Point Clouds. *ISPRS Int. Arch. Photogramm. Sens. Spat. Inf. Sci.* **2016**, *XLI-B5*, 799–804. [CrossRef]
18. Dershowitz, W.S.; Herda, H.H. Interpretation of fracture spacing and intensity. In Proceedings of the 33rd US Symposium on Rock Mechanics, Santa Fe, NM, USA, 3–5 June 1992; pp. 757–766.
19. Francioni, M.; Salvini, R.; Stead, D.; Litrico, S. A case study integrating remote sensing and distinct element analysis to quarry slope stability assessment in the Monte Altissimo area, Italy. *Eng. Geol.* **2014**, *183*, 290–302. [CrossRef]
20. Oniga, V.-E.; Breaban, A.-I.; Stătescu, F. Determining the Optimum Number of Ground Control Points for Obtaining High Precision Results Based on UAS Images. *Proceedings* **2018**, *2*, 352. [CrossRef]
21. Novakova, L.; Pavlis, T.L. Assessment of the precision of smart phones and tablets for measurement of planar orientations: A case study. *J. Struct. Geol.* **2017**, *97*, 93–103. [CrossRef]
22. Haneberg, W.C. Directional roughness profiles from three-dimensional photogrammetric or laser scanner point clouds. In Proceedings of the 1st Canada-U.S. Rock Mechanics Symposium, Vancouver, BC, Canada, 27–31 May 2007; pp. 101–106.
23. Poropat, G. Remote characterisation of surface roughness of rock discontinuities. In *1st Southern Hemisphere International Rock Mechanics Symposium*; Australian Centre for Geomechanics: Perth, Australia, 2008.

24. Kim, D.H.; Gratchev, I.; Balasubramaniam, A. Determination of joint roughness coefficient (JRC) for slope stability analysis: A case study from the Gold Coast area, Australia. *Landslides* **2013**, *10*, 657–664. [CrossRef]
25. Tong, X.; Liu, X.; Chen, P.; Liu, S.; Luan, K.; Li, L.; Liu, S.; Liu, X.; Xie, H.; Jin, Y.; et al. Integration of UAV-Based Photogrammetry and Terrestrial Laser Scanning for the Three-Dimensional Mapping and Monitoring of Open-Pit Mine Areas. *Remote Sens.* **2015**, *7*, 6635–6662. [CrossRef]
26. Caporossi, P.; Mazzanti, P.; Bozzano, F. Digital Image Correlation (DIC) Analysis of the 3 December 2013 Montescaglioso Landslide (Basilicata, Southern Italy): Results from a Multi-Dataset Investigation. *ISPRS Int. J. GeoInf.* **2018**, *7*, 372. [CrossRef]
27. Wu, C. VisualSFM: A Visual Structure from Motion System. 2011. Available online: http://www.cs.washington.edu/homes/ccwu/vsfm/ (accessed on 2 July 2018).